Nodulin Intrinsic Protein 7;1 Is a Tapetal Boric Acid Channel Involved in Pollen Cell Wall Formation[1][OPEN]

Pratyush Routray,[a,2] Tian Li,[a,2,3] Arisa Yamasaki,[b] Akira Yoshinari,[b,4] Junpei Takano,[b] Won Gyu Choi,[a,5] Carl E. Sams,[c] and Daniel M. Roberts[a,6,7]

[a]Department of Biochemistry and Cellular and Molecular Biology and Program in Genome Science and Technology, University of Tennessee, Knoxville, Tennessee 37996
[b]Graduate School of Life and Environmental Sciences, Osaka Prefecture University, Sakai-shi, Osaka 599-8531, Japan
[c]Department of Plant Sciences, University of Tennessee Institute of Agriculture, Knoxville, Tennessee 37996

ORCID IDs: 0000-0002-7474-3101 (J.T.); 0000-0002-0113-9376 (W.G.C.); 0000-0002-0780-7056 (D.M.R.)

Boron is an essential plant micronutrient that plays a structural role in the rhamnogalacturonan II component of the pectic cell wall. To prevent boron deficiency under limiting conditions, its uptake, distribution, and homeostasis are mediated by boric acid transporters and channel proteins. Among the membrane channels that facilitate boric acid uptake are the type II nodulin intrinsic protein (NIP) subfamily of aquaporin-like proteins. Arabidopsis (*Arabidopsis thaliana*) possesses three NIP II genes (*NIP5;1*, *NIP6;1*, and *NIP7;1*) that show distinct tissue expression profiles (predominantly expressed in roots, stem nodes, and developing flowers, respectively). Orthologs of each are represented in all dicots. Here, we show that purified and reconstituted NIP7;1 is a boric acid facilitator. By using native promoter-reporter fusions, we show that NIP7;1 is expressed predominantly in anthers of young flowers in a narrow developmental window, floral stages 9 and 10, with protein accumulation solely within tapetum cells, where it is localized to the plasma membrane. Under limiting boric acid conditions, loss-of-function T-DNA mutants (*nip7;1-1* and *nip7;1-2*) show reduced fertility, including shorter siliques and an increase in aborted seeds, compared with the wild type. Under these conditions, *nip7;1* mutant pollen grains show morphological defects, increased aggregation, defective exine cell wall formation, reduced germination frequency, and decreased viability. During stages 9 and 10, the tapetum is essential for supplying materials to the pollen microspore cell wall. We propose that NIP7;1 serves as a gated boric acid channel in developing anthers that aids in the uptake of this critical micronutrient by tapetal cells.

[1]This work was supported by National Science Foundation Grants MCB-0618075 and MCB-1121465.

[2]These authors contributed equally to the article.

[3]Current address: Department of Biochemistry and Molecular Biology, University of Chicago, Chicago, IL 60637.

[4]Current address: Institute of Transformative Biomolecules, Nagoya University, Furo-cho, Chikusa, Nagoya 464-8601, Japan.

[5]Current address: Department of Biochemistry and Molecular Biology, University of Nevada, Reno, NV 89557.

[6]Address correspondence to drobert2@utk.edu.

[7]Senior author.

The author responsible for distribution of materials integral to the findings presented in this article in accordance with the policy described in the Instructions for Authors (www.plantphysiol.org) is: Daniel M. Roberts (drobert2@utk.edu).

P.R., together with T.L., designed and executed the majority of the experiments and was the major writer of the article; T.L. performed a majority of the early experiments and, along with P.R., was the major contributor to the experimental content of the work; Ar.Y. and Ak.Y. generated and performed the localization experiments with NIP7;1-GFP constructs; J.T., together with D.M.R., planned the scope of the study and supervised the localization experiments; W.G.C. initiated the project and generated the reporter constructs and T-DNA lines used in the work; C.E.S. and P.R. designed and conducted the ICP-MS experiments; D.M.R., supervisor of the project, conceived the project and was involved in the design of experiments, analysis, and interpretation of the data and, along with P.R., was the major writer of the article.

[OPEN]Articles can be viewed without a subscription.
www.plantphysiol.org/cgi/doi/10.1104/pp.18.00604

The aquaporin superfamily consists of integral membrane protein channels that facilitate the transport of water and other uncharged solutes across cellular membranes (Chaumont and Tyerman, 2014; Maurel et al., 2015). The nodulin 26-like intrinsic proteins (NIPs) constitute a plant-specific subfamily of the aquaporin superfamily that is named for the archetype of the family, nodulin 26, which was demonstrated originally in nitrogen-fixing soybean (*Glycine max*) root nodules (Fortin et al., 1987). NIPs appeared early in land plant evolution and have undergone substantial structural and functional diversification (Danielson and Johanson, 2010; Abascal et al., 2014; Roberts and Routray, 2017). As a result, while they possess the basic structural fold of the aquaporin superfamily, they have a broad array of biological and biochemical functions and transport an array of substrates besides water, including metalloid hydroxides (boric acid, arsenous acid, and others), glycerol, lactic acid, urea, and hydrogen peroxide (Ludewig and Dynowski, 2009; Pommerrenig et al., 2015; Roberts and Routray, 2017). In seed plants, structural modeling and phylogenetic analysis of NIPs show that they can be grouped into three pore families (NIP I, II, and III) based on the composition of the four amino acids forming the selectivity filter of the pore (ar/R region; Wallace and Roberts, 2004; Danielson and Johanson, 2010; Mitani-Ueno et al., 2011; for review, see Roberts and Routray, 2017). Substantial genetic and

biochemical evidence show that proteins of the NIP II subfamily serve as permeases of boric acid (Takano et al., 2006, 2008; Tanaka et al., 2008; Miwa and Fujiwara, 2010; Hanaoka et al., 2014; Pommerrenig et al., 2015; Bienert and Bienert, 2017; Yoshinari and Takano, 2017).

Boron (B) is an essential plant micronutrient (Dell and Huang, 1997; Camacho-Cristóbal et al., 2008) with a role in cell wall structure/function and development by providing borate cross-linking of the rhamnogalacturonan II (RG-II) pectin cell wall (O'Neill et al., 2004). Under conditions of soil and physiological pH, B is found principally as boric acid, a weak, uncharged Lewis acid (Kot, 2009). While boric acid permeates lipid bilayers, it exhibits limited systemic mobility within most plant species (Shelp et al., 1995), including Arabidopsis (*Arabidopsis thaliana*; Takano et al., 2001), which contributes to B deficiency under low soil boric acid concentrations. Conversely, while boric acid is an essential plant micronutrient, the maintenance of its cellular concentration is critical, since it is toxic at high concentrations (Camacho-Cristóbal et al., 2008). As a result, boric acid uptake, distribution, and homeostasis are tightly regulated by the expression and spatial localization of NIP proteins and secondary transporters of the *BOR* family to coordinate the directional transport of boric acid to tissues of need (for review, see Takano et al., 2008; Miwa and Fujiwara, 2010; Yoshinari and Takano, 2017).

The Arabidopsis NIP subfamily contains nine genes (Johanson et al., 2001) with three genes representing the NIP II subgroup: *NIP5;1*, *NIP6;1*, and *NIP7;1* (Wallace and Roberts, 2004). *NIP5;1* is a root-specific transcript (Takano et al., 2006), whereas *NIP6;1* is expressed in a shoot-specific manner, particularly within the phloem vascular tissue of young developing leaf nodes (Tanaka et al., 2008). The expression of *NIP5;1* and *NIP6;1* is induced by the limitation of boric acid in the growth medium, and both show boric acid channel activity upon expression in *Xenopus laevis* oocytes (Takano et al., 2006; Tanaka et al., 2008). *NIP5;1* and *NIP6;1* T-DNA mutants show developmental defects that are sensitive to B deficiency, including gross reduction in cell elongation and tissue expansion, particularly in young developing organs (Takano et al., 2006; Tanaka et al., 2008).

While the NIP II proteins NIP5;1 and NIP6;1 are established boric acid facilitators with tissue/organ-specific localization to the roots and young leaf nodes, less is known about the biological function of NIP7;1. Previous work shows that NIP7;1 is expressed preferentially in flower tissues (Li et al., 2011). Given the particular sensitivity of microsporogenesis and pollen development to B limitation (Huang et al., 2000) and the reproductive phenotypes observed with T-DNA mutations of BOR transporters (Noguchi et al., 1997; Tanaka et al., 2013), it has been postulated that NIP7;1 may play a role in B homeostasis during flower development, although the rate of boric acid transport of the wild-type protein in *X. laevis* oocytes was extremely low (Li et al., 2011).

In this study, the solute and water permeability properties of purified and reconstituted NIP7;1 were quantified by stopped flow fluorimetry, and its function as a boric acid permease is demonstrated. Furthermore, it is demonstrated that NIP7;1 is expressed predominantly as a plasma membrane protein in the anther tapetum of stage 9 and 10 flowers. The analysis of *nip7;1* mutants shows B-dependent defects in fertility and defective pollen exine cell wall architecture, suggesting a role for the protein in cell wall biosynthesis during microsporogenesis and pollen grain development.

RESULTS

Purified and Reconstituted NIP7;1 Transports Boric Acid in a Water-Tight Fashion

Despite its structural similarity to NIP5;1 and NIP6;1 within pore determinant regions, previous work with NIP7;1 in *X. laevis* oocytes showed that it differed from these two proteins and exhibited the apparent absence of boric acid permeability (Li et al., 2011). Boric acid permeability could be restored by mutagenesis of a proposed gating residue (Tyr-81), but the boric acid permeability properties of wild-type NIP7;1 are still unclear.

To quantify and determine more precisely the solute and water permeability properties of NIP7;1, a strategy for expression, purification, and reconstitution into liposomes was adopted (Dean et al., 1999; Hwang et al., 2010). NIP7;1 was expressed as a His-tagged recombinant protein in *Pichia pastoris* and was purified by nickel-chelate chromatography (Fig. 1A). To evaluate and quantify the solute and water permeabilities of NIP7;1, an established stopped-flow fluorimetric assay for the transport of nonelectrolytes (Rivers et al., 1997; Dean et al., 1999) was employed with carboxyfluorescein-loaded NIP7;1 proteoliposomes (Fig. 1; Supplemental Fig. S1). Reconstitution of NIP7;1 into proteoliposomes resulted in the acquisition of enhanced boric acid permeability that is statistically higher than the diffusive rate in negative control liposomes (Figs. 1B and 2A). After correction for the nonselective rate of diffusion through the lipid bilayer, the boric acid permeability coefficient (P_B) for the NIP7;1 channel was estimated as follows: $P_B = 1.41 \times 10^{-6} \pm 0.18$ cm s^{-1}.

Similar to other NIP II proteins (Wallace and Roberts, 2005), NIP7;1 also is permeable to glycerol (Fig. 1D). However, NIP7;1 shows an approximate 6-fold preference for boric acid over glycerol ($k_{glycerol} = 0.083\ s^{-1}$, $k_{boric\ acid} = 0.46\ s^{-1}$). A characteristic feature of NIP II permeases is that they show little to no aquaporin activity (Roberts and Routray, 2017). Analysis of the osmotic water permeability of NIP7;1 proteoliposomes by stopped-flow fluorimetry shows that it is no higher than the bare bilayer diffusion rate of negative control liposomes (Fig. 1C). Thus, NIP7;1 is a water-tight boric acid permease that also fluxes glycerol, albeit at a lower rate.

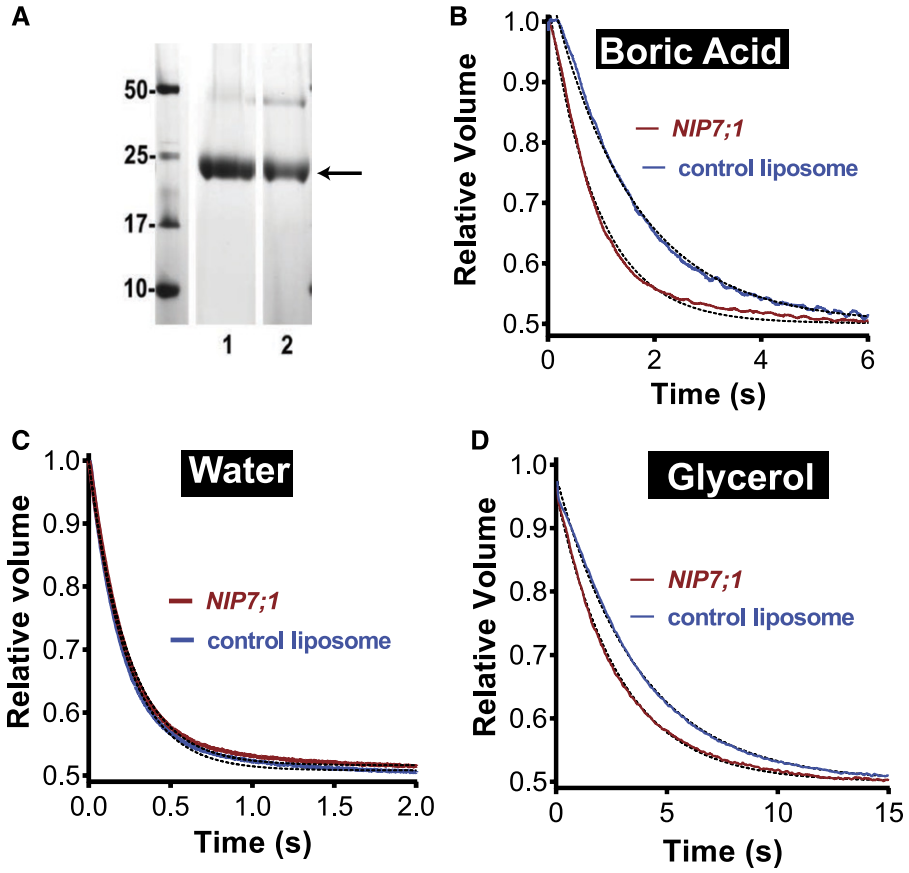

Figure 1. Solute and water permeability of NIP7;1 in reconstituted proteoliposomes. A, SDS-PAGE profile of recombinant NIP7;1 proteins purified from *P. pastoris*. Proteins were resolved by SDS-PAGE on a 12% (w/v) polyacrylamide gel and stained with Coomassie Blue. Lane 1, NIP7;1; lane 2, NIP7:1Y81C. The band corresponding to the monomer molecular mass is indicated with the arrow. A second band characteristic of a dimeric form of the protein, often observed with purified aquaporin-like proteins, is apparent at 50 kD. B to D, Permeability measurements of the indicated solutes or water were conducted by stopped-flow fluorimetry as described in "Materials and Methods" (the rationale is shown in Supplemental Fig. S1). Shown are fluorescence traces from negative control liposomes and NIP7;1 proteoliposomes that represent an average of 10 determinations fit to a single exponential decay.

The strong P_B exhibited by purified NIP7;1 proteoliposomes contrasts with the results obtained with NIP7;1 expressed in *X. laevis* oocytes, which show extremely low boric acid transport rates that are statistically indistinguishable from those of negative control oocytes (contrast Fig. 2, A and B). Homology modeling of NIP7;1 shows that, unlike other NIP boric acid permeases, the protein possesses a conserved Tyr in helix 2 (Y81) that can serve as a gate that reversibly blocks the pore (Li et al., 2011). Molecular dynamics simulations produce models in which Y81 can exist in two rotomeric states: up (open) or down (closed) state (Fig. 2C). Docking of a transport substrate (e.g. glycerol; Fig. 2C) shows that Tyr in the down state would sterically block the access of the ar/R region. Replacement of Tyr with a small side chain amino acid (e.g. NIP7;1Y81C, in which Tyr is replaced with Cys that is characteristic of NIP6;1) opens the pore to boric acid permeability in *X. laevis* oocytes (Fig. 2B). Comparison of NIP7;1Y81C and NIP7;1 proteoliposomes (Fig. 2B) shows that, while the Y81C mutant shows higher boric acid permeability ($P_B = 2.82 \times 10^{-6} \pm 0.078$ cm s^{-1}), the differences fall short of statistical significance ($P = 0.065$). Nevertheless, the data show that NIP7;1 is active (open) in proteoliposomes and inactive (closed) in *X. laevis* oocytes. The observation that NIP7;1Y81C is open in both proteoliposomes and oocytes, together with the molecular dynamics and docking data, suggest that Tyr-81 is responsible for this different behavior. The factors that control the preference of NIP7;1 for an open or closed state remain to be elucidated.

NIP7;1 Is Localized to the Plasma Membrane of Tapetal Cells in a Narrow Developmental Window in Developing Anthers

Previous reverse transcription (RT) quantitative PCR data showed that *NIP7;1* is expressed preferentially in flower tissues, with lower levels also found in siliques and roots (Li et al., 2011). GUS staining of *NIP7;1pro*::*GUS* reporter plants supports this previous result, with *NIP7;1pro*::*GUS* plants showing the most intense GUS staining in the inflorescence, particularly in young flowers, and a lower degree of staining within the root tip and stele (Supplemental Fig. S2). Closer examination of the individual flowers (Fig. 3A) shows that *NIP7;1* promoter activity based on GUS staining is first detected at floral stage 8, peaks within stages 9 and 10, and declines thereafter and completely disappears by stage 12. Within individual flowers, GUS staining is detected only in anthers. Cross sections of *NIP7;1pro*::*GUS* stage 9 and 10 flowers show GUS staining in pollen microspores as well as in the surrounding tapetum (Fig. 3, B–D).

To investigate the expression and cellular localization of NIP7;1 protein, transgenic lines expressing NIP7;1 with an in-frame C-terminal yellow fluorescent protein

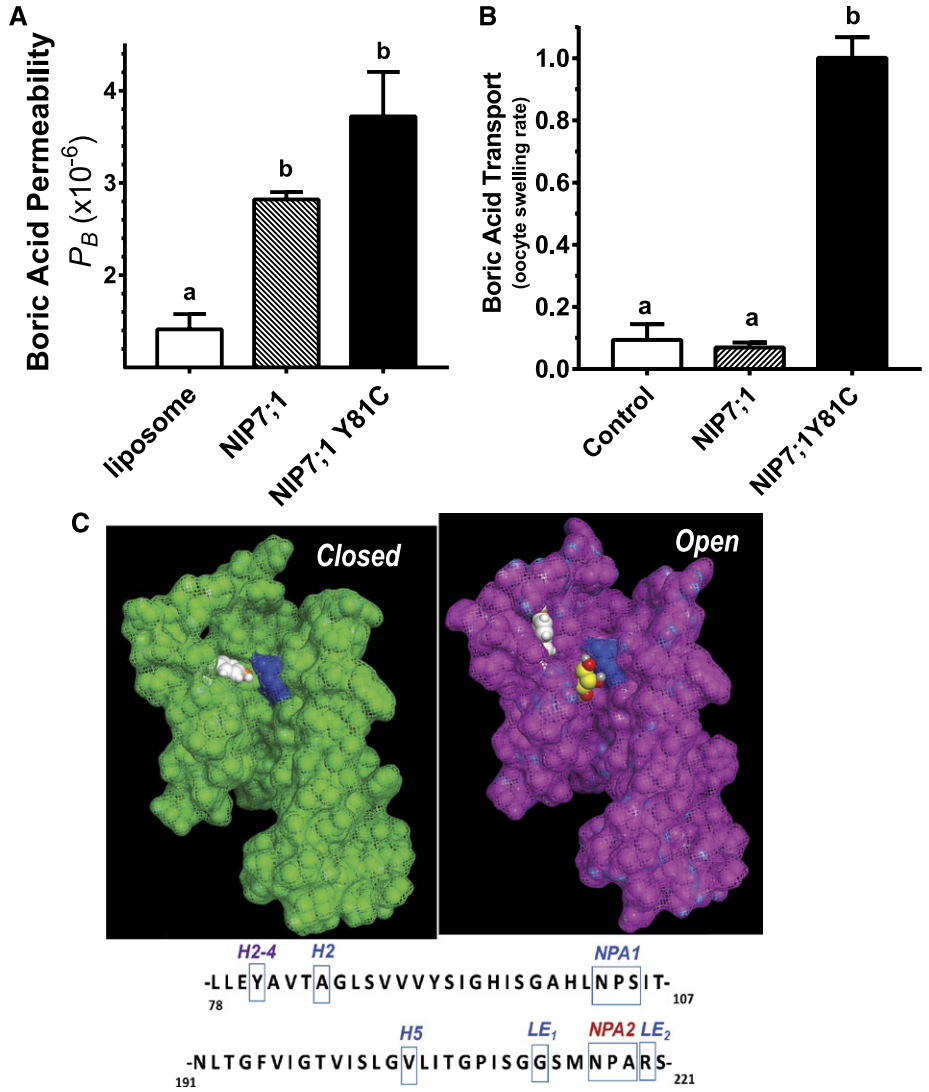

Figure 2. Effect of NIP7;1 Tyr-81 on boric acid permeability. A, P_B of NIP7;1 and NIP7;1Y81C proteoliposomes and negative control liposomes were calculated from the stopped-flow fluorimetric data as described in "Materials and Methods." The error bars show SE (n = 3 liposome preparations). B, Comparative boric acid permeability of NIP7;1 and NIP7;1Y81C expressed in *X. laevis* oocytes based on a swelling assay (Wallace and Roberts, 2005; Tanaka et al., 2008). Control represents the swelling rate of negative control oocytes injected with sterile water. The error bars show SE (n = 4 oocytes). Different letters above the histograms in A and B indicate statistically significant differences based on multiple comparison analysis by one-way ANOVA (Tukey's test). C, Homology models showing the pore structures of the closed (green) and open (magenta) states of the NIP7;1 monomer shown with space-filling atoms and a van der Waals surface. Helix 4 (residues 150–190) and part of the second NPA helix (residues 207–216) were removed to highlight the position of the conserved Arg in LE_2 of the ar/R selectivity filter (shown in blue) and the Tyr gating residue at the H2-4 position (shown in white). In the open state, a docked glycerol molecule is shown in yellow with hydroxyl groups in red. Glycerol and boric acid adopt similar trihydoxylated structures (Supplemental Fig. S1), and NIP II channels are permeated by both substrates (Wallace and Roberts, 2005). Sequences of Arabidopsis NIP7;1 annotated with the location of the NPA boxes, the four residues of the ar/R selectivity region, and the conserved Tyr in helix 2 are shown below the models.

tag (*NIP7;1-3xYFP*) were produced using recombineering technology (Zhou et al., 2011). This approach allows in situ YFP tagging of the protein encoded by the gene of interest within bacterial artificial chromosome clones that contain the larger genomic context (Zhou et al., 2011). Similar to the results of *promoter::GUS* experiments, western-blot analysis of extracts from dissected flowers of defined developmental stages from *NIP7;1-3YFP* recombineering lines showed maximal expression within floral stages 9 and 10 (Fig. 4A). This is supported by confocal fluorescent microscopic analysis that shows the highest levels of NIP7;1-YFP signal in anthers of stage 9 and 10 flowers, a decline in signal at stage 11, and a nearly complete loss of signal in the anthers of stage 12 flowers as the pollen grains mature and the tapetum degenerates (Fig. 4B). Finer examination

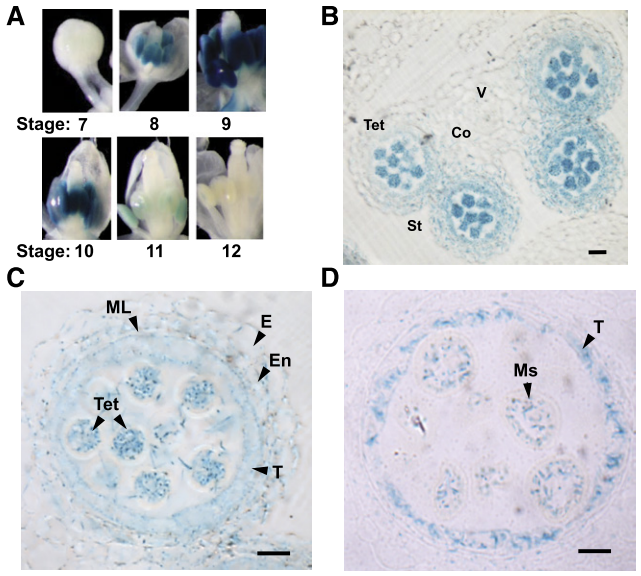

Figure 3. Expression of AtNIP7;1 in developing Arabidopsis flowers. A, Analysis of GUS expression in dissected flowers of 6-week-old transgenic plants expressing the *NIP7;1pro*::*GUS* construct. Floral stages based on the nomenclature of Smyth et al. (1990) are indicated. B, Anther cross section from late floral stage 9 (anther stage 7) with released tetrad microspores. Co, Connective; St, stomium; Tet, microspore tetrads; V, vascular region. Bar = 20 μm. C and D, Comparison of the GUS staining pattern in microsporangia from late floral stage 9 with tetrad microspores surrounded by callose cell wall (C) and floral stage 10 with separated microspores (D). E, Epidermis; En, endothecium; ML, middle layer; Ms, released single microspores; T, tapetum; Tet, tetrad. Bars = 10 μm.

of fixed flower samples revealed that the YFP signal is localized specifically and solely to the anther tapetal cells (Fig. 4C).

To determine the subcellular localization of the protein, an Arabidopsis line harboring a construct of *NIP7;1* fused to a single copy of monomeric GFP (Segami et al., 2014) driven by the native *NIP7;1* promoter was generated. Examination of NIP7;1-GFP in anther tissues from stage 9 flowers shows that the fluorescent signal is limited to the tapetum with no apparent signal detected in the microspores (Fig. 5). NIP7;1 shows plasma membrane localization at the cell surface between adjacent tapetal cells and, thus, similar to previous observations with the NIP II proteins NIP5;1 (Takano et al., 2006, 2010; Wang et al., 2017) and NIP6;1 (Tanaka et al., 2008), appears to localize to the plasma membrane. NIP7;1 fluorescence also is detected within intracellular structures as well (Fig. 5), including some punctate fluorescence bodies within the cytosol.

Overall, the results show that *NIP7;1* is expressed in a tightly controlled developmental window during male gametogenesis that peaks during microsporogenesis (floral stages 9 and 10), declines during the pollen mitotic divisions (floral stage 11), and is no longer detectable when tricellular pollen maturation is complete and anther dehiscence occurs (floral stages 12–14). Although the promoter activity suggests gene expression in both developing microspore and tapetal cells, translational fusions of NIP7;1 driven by the native promoter show that expression is detected only in tapetal cells, with peak expression in stage 9 and 10 flowers, suggesting that NIP7;1 is a tapetum-localized protein at these developmental stages.

Loss-of-Function *nip7;1* T-DNA Insertional Mutants Show B-Dependent Sterility and Defective Pollen

Since NIP7;1 is a boric acid-permeable channel (Fig. 1), the working hypothesis is that the protein plays a role as a B permease during anther development in stage 9 to 11 flowers. To address its potential biological function, two independent T-DNA lines with insertions in the fourth exon (SALK_042590; *nip7;1-1*) and the second intron (SALK_057023; *nip7;1-2*) of *NIP7;1* were characterized (Supplemental Fig. S3). PCR genotyping verified that both lines were homozygous for the T-DNA insert, and the loss of *NIP7;1* transcripts in 6-week-old Arabidopsis flowers was confirmed by RT-PCR (Supplemental Fig. S3).

Previous work with Arabidopsis NIP5;1 and NIP6;1 boric acid permeases showed that T-DNA mutants do not show phenotypes unless grown under boric acid-deficient conditions (Takano et al., 2006; Tanaka et al., 2008). Similar to these observations, the *nip7;1* mutants showed little difference from wild-type controls with respect to vegetative and reproductive growth under standard growth conditions with an adequate boric acid concentration (60 μM). To determine whether *nip7;1* mutants displayed developmental defects under limiting B, plants were grown hydroponically under standard conditions (60 μM boric acid) for 21 d and then were transferred to medium containing either adequate (100 μM) or limiting (0.3 μM) boric acid, with growth continued through flowering, silique development, and seed set.

Under normal B concentrations, silique development of wild-type, *nip7;1-1*, and *nip7;1-2* plants was indistinguishable, with each showing fully elongated siliques and normal seed fill (Fig. 6). Under reduced B concentrations, wild-type and mutant plants showed no detectable differences in vegetative growth (Supplemental Fig. S4) and exhibited similar flowering times and flower development. This is in contrast to *nip5;1* and *nip6;1* T-DNA mutants, which show severe vegetative developmental phenotypes under low-B conditions (Takano et al., 2006; Tanaka et al., 2008). The major phenotype observed in *nip7;1* plants under limiting B is within developmental tissues, with significant differences observed between the size of siliques of wild-type and *nip7;1* mutant plants (Fig. 6). Under these conditions, over 40% of siliques of *nip7;1-1* and *nip7;1-2* plants show severely stunted growth (less than 0.5 cm in length). In addition, *nip7;1-1* and *nip7;1-2* plants exhibited evidence of seed abortion and reduced seed set (Fig. 6), which was not observed in wild-type siliques. These observations suggest that *nip7;1* mutants show compromised fertility under limiting B conditions.

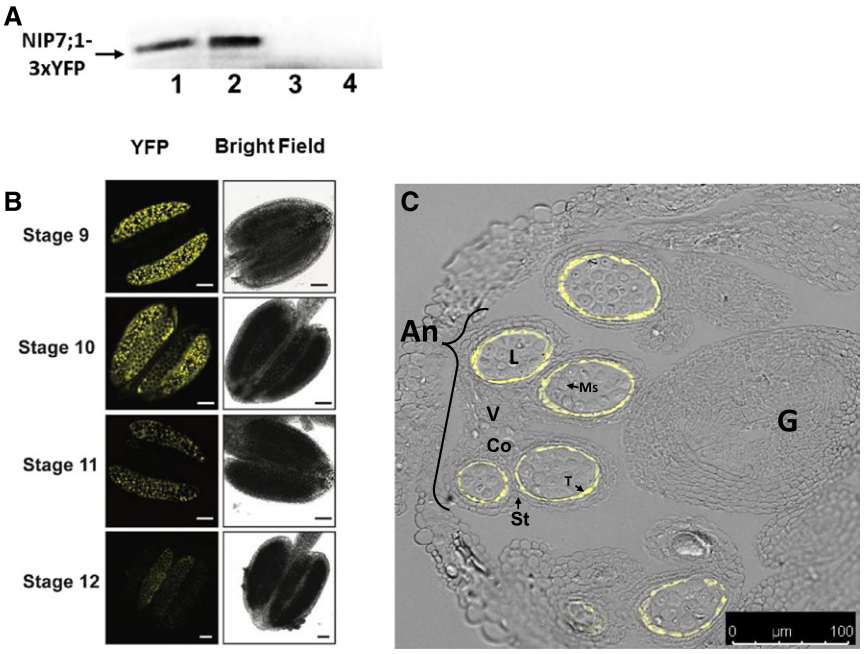

Figure 4. Localization of AtNIP7;1 protein in developing Arabidopsis anthers. A, Western-blot analysis of AtNIP7;1 from extracts (10 µg of extract protein per lane) of dissected Arabidopsis flower buds at the following stages: lane 1, stages 9 and 10; lane 2, stages 10 and 11; lane 3, stage 12; and lane 4, stages 13 and 14. The arrow indicates the position (100 kD) expected for the NIP7;1-3xYFP protein product. B, Confocal fluorescence micrographs of live anthers of *NIP7;1*:*3xYFP* recombineering plants at the indicated floral stages. Bars = 50 µm. C, Confocal fluorescence micrograph of an anther section from a stage 10 flower (anther stage 9) of *NIP7;1*:*3xYFP* recombineering plants superimposed on a differential interference contrast image of an anther with various cell types indicated. An, Anther; Co, connective; G, gynoecium; L, locule; Ms, pollen microspores; St, stomium; T, tapetum; V, vascular region. Bar = 50 µm.

Shortened siliques and abortion of seed development is a phenotype that is commonly observed in Arabidopsis mutants with defective male gametophyte and pollen development that lead to reduced fertility (Vivian-Smith et al., 2001). Given the selective expression of *NIP7;1* in tapetum cells in the critical developmental stages that span microsporogenesis and pollen cell wall formation (floral stages 9–11), it was hypothesized that seed abortion and reduced seed set could be the result of defective pollen development. The pollen viability and germination properties were assessed for *nip7;1* mutant pollen obtained under normal- and low-B growth conditions (Fig. 7). In vitro germination frequencies of pollen from wild-type and *nip7;1* flowers obtained under normal B showed no significant differences (Fig. 7A). In contrast, the germination frequency of pollen obtained from *nip7;1* flowers under low-B conditions showed a substantial reduction in germination compared with wild-type controls.

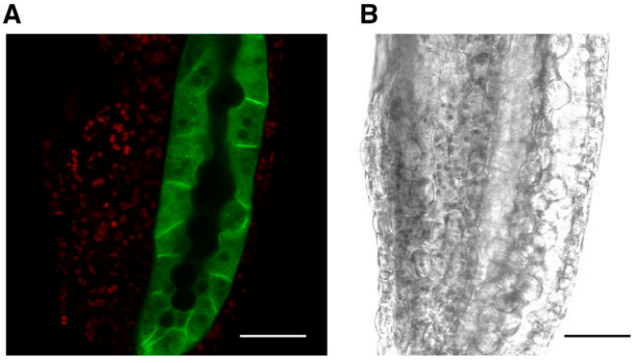

Figure 5. Subcellular localization of NIP7;1 in tapetal cells. A, Confocal micrograph of a representative anther (stage 9 flower, anther stage 6, vacuolated tapetum based on Sanders et al. [1999]) from *NIP7;1pro*::*NIP7;1-GFP* plants in the *nip7;1-2* background. The GFP signal (green) is superimposed on the chlorophyll autofluorescence signal (red). B, Differential interference contrast image. Bars = 30 µm.

Investigation of the viability of wild-type and mutant pollen from flowers from plants cultured under limiting B by staining with the cell-permeable vital dye fluorescein diacetate showed a higher incidence of nonviable *nip7;1* pollen grains as well as a number of pollen grains with irregular morphology (Fig. 8B). Closer examination of wild-type and mutant pollen by scanning electron microscopy (SEM) shows that, under normal-B conditions, *nip7;1* pollen was largely indistinguishable from wild-type pollen, exhibiting the characteristic reticulate pattern (Scott et al., 2004) of the external tectate exine cell wall with well-defined lacuna apertures (Fig. 8A). However, under limiting-B conditions, over 60% of the *nip7;1* pollen grains exhibited defects in the morphology of the exine cell wall and in cellular shape (Fig. 8B). These include breaks in the exine reticulate structure, regions of poorly formed exine cell wall with occluded lacuna, and aggregates of poorly developed pollen grains (Fig. 8C). Comparison of wild-type and defective *nip7;1* pollen by transmission electron microscopy (TEM) showed a poorly developed outer (sexine) exine cell wall in the mutant (Supplemental Fig. S5). These data show that NIP7;1 is a tapetum plasma membrane boric acid permease and suggest that it is essential for the structural development of the pollen exine cell wall.

DISCUSSION

B is a critical micronutrient essential for normal plant growth and development (Dell and Huang, 1997;

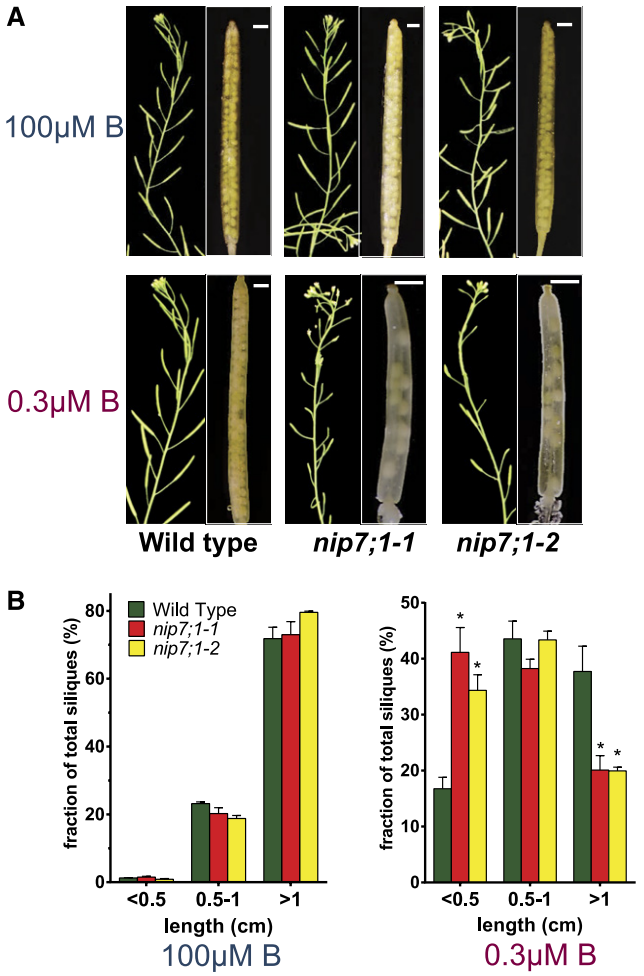

Figure 6. Siliques of wild-type, *nip7;1-1*, and *nip7;1-2* plants grown under limiting and adequate boric acid growth conditions. A, Siliques from 6-week-old plants grown hydroponically in medium containing 100 and 0.3 μM boric acid. Short siliques with aborted seeds were identified only in *nip7;1-1* and *nip7;1-2* plants under low-boric acid conditions. The *nip7;1-1* and *nip7;1-2* siliques under low-B conditions are magnified at right to illustrate the presence of aborted seeds. Bars = 1 mm. B, Silique length distributions are shown for wild-type (green bars), *nip7;1-1* (red bars), and *nip7;1-2* (yellow bars) plants grown under 100 μM (left) and 0.3 μM (right) boric acid conditions. The error bars show SE for three biological replicates, with each replicate representing 200 to 500 siliques. Asterisks denote significance by Student's *t* test compared with wild-type plants: $P < 0.01$.

Blevins and Lukaszewski, 1998; Goldbach et al., 2007; Camacho-Cristóbal et al., 2008), with reproductive tissues showing particular sensitivity to B deficiency (Dell et al., 2002). A collection of boric acid transporters and channels have evolved to facilitate the uptake and directional transport of boric acid to sink tissues of need (Takano et al., 2008; Miwa and Fujiwara, 2010; Yoshinari and Takano, 2017). Plants possess two types of B-permeable transport proteins: (1) the *BOR* family of secondary transporters, which mediate the efflux of borate ions; and (2) NIPs, particularly those of the NIP II pore subclass, which are boric acid channels that facilitate the passive transmembrane flux of uncharged boric acid driven by transmembrane concentration gradients. In this study, evidence is presented that the NIP II protein NIP7;1 is a tapetum-localized boric acid channel that plays a role in pollen cell wall development in Arabidopsis.

NIP7;1 Is a Boric Acid Permease with Unusual Properties

The diversification of the *NIP* gene family during vascular plant evolution resulted in the emergence of three structural pore families: NIP I, NIP II, and NIP III (for review, see Roberts and Routray, 2017). Each pore family possesses conserved signature sequences and structures within the ar/R selectivity filter as well as distinct substrate selectivity profiles (Wallace and Roberts, 2004, 2005; Liu and Zhu, 2010; Mitani-Ueno et al., 2011; Roberts and Routray, 2017). NIP II and NIP III channels have wider ar/R regions than NIP I proteins and are involved in the transport of uncharged metalloid nutrients: boric acid (NIP II proteins) and silicic acid (NIP III proteins; Ma and Yamaji, 2006, 2015; Takano et al., 2006; Mitani et al., 2008; Tanaka et al., 2008; Miwa et al., 2010; Mitani-Ueno et al., 2011) as well as a number of additional metalloid hydroxides (Pommerrenig et al., 2015; Bienert and Bienert, 2017).

Like most dicots, Arabidopsis lacks members of the NIP III subgroup but possesses three genes (*NIP5;1*, *NIP6;1*, and *NIP7;1*) encoding NIP II proteins. Phylogenetic analysis of the NIP II proteins across a wide array of dicot species reveals segregation into NIP5;1, NIP6;1, and NIP7;1 clades (Fig. 9), with NIP7;1 proteins showing greater evolutionary divergence from the other two NIP II groups (Roberts and Routray, 2017). While other NIP II proteins are present in early plant lineages, NIP7;1 proteins are found only in dicot species (Supplemental Table S1), suggesting that they evolved more recently (Roberts and Routray, 2017).

In addition to these differences between NIP6;1 and NIP5;1 proteins, NIP7;1 shows complexity in boric acid permeability. Transport analysis of NIP7;1 in *X. laevis* oocytes reveals a boric acid channel with low intrinsic permeability (Li et al., 2011). In this study, the permeability of the NIP7;1 channel was investigated quantitatively by stopped-flow fluorimetry with proteoliposomes containing reconstituted, purified NIP7;1. The results indicate that wild-type NIP7;1 is a boric acid permease with a P_B that is significantly higher than the diffusive permeability through control lipid bilayers. Furthermore, similar to other NIP II proteins (Wallace and Roberts, 2005), NIP7;1 (1) also is a glycerol permease, albeit with a severalfold lower $P_{glycerol}$ compared with P_B; and (2) completely lacks detectable aquaporin activity (i.e. is water tight). Comparison of glycerol with boric acid (Supplemental Fig. S1) shows that both have a trihydroxylated structure and a similar molecular volume. Furthermore, quantum calculations show that, in solution, glycerol (which is sterically less constrained than the trigonal boric acid structure) can

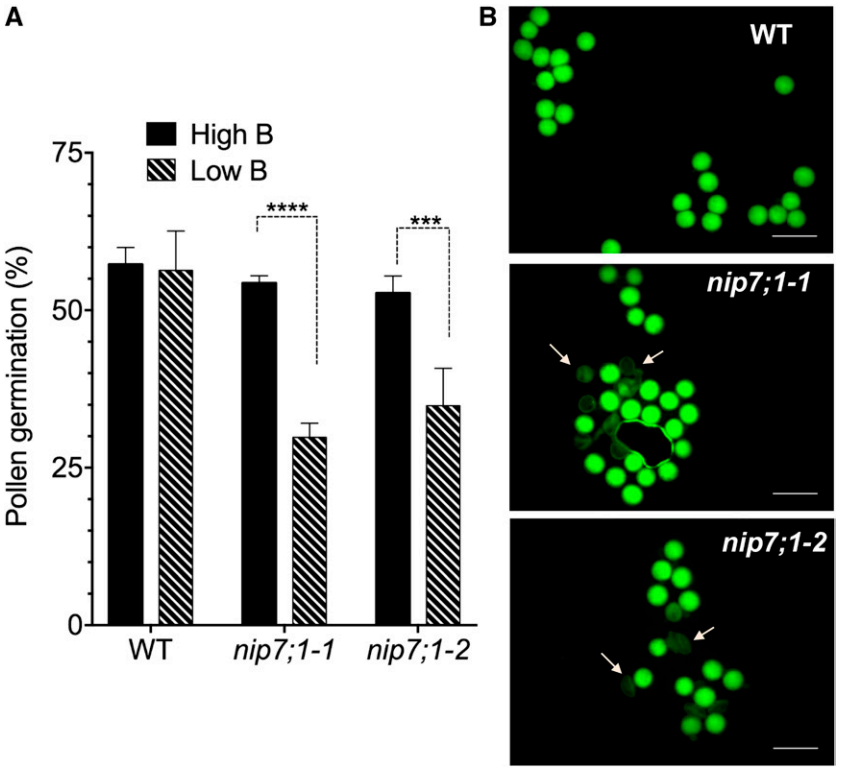

Figure 7. Viability and germination frequency of *nip7;1* pollen. Pollen harvested from flowers of the wild type (WT) and *nip7;1* T-DNA mutant lines were tested for viability and germination in vitro as described in "Materials and Methods." A, The percentage of geminated pollen was calculated after 16 h of incubation of pollen in pollen growth medium. Error bars show SD (n = 5, with 60–200 pollen grains per replicate). Significant differences (***, $P < 0.001$ and ****, $P < 0.0001$) based on two-way ANOVA are indicated. B, Pollen viability was tested by staining mature pollen from plants grown hydroponically in low-boric acid medium with cell-permeable fluorescein diacetate. The hydrolysis of fluorescein diacetate within viable pollen grains produces a green fluorescent signal detected with a fluorescein isothiocyanate filter set. Arrows show characteristic defective pollen grains detected in *nip7;1* pollen. Bars = 50 µm.

occupy over 500 conformations, including a small subset of retracted conformations that show similarity in structure (orientation of hydrogen-bonding hydroxyl groups, electrostatic potential, and molecular volume) to boric acid-like metalloid hydroxides (Porquet and Filella, 2007). Thus, an interesting possibility is that boric acid permeases have their origin as aquaporin-like glycerol transporters.

The reason for the discrepancy between the *X. laevis* results and the proteoliposome data could be explained

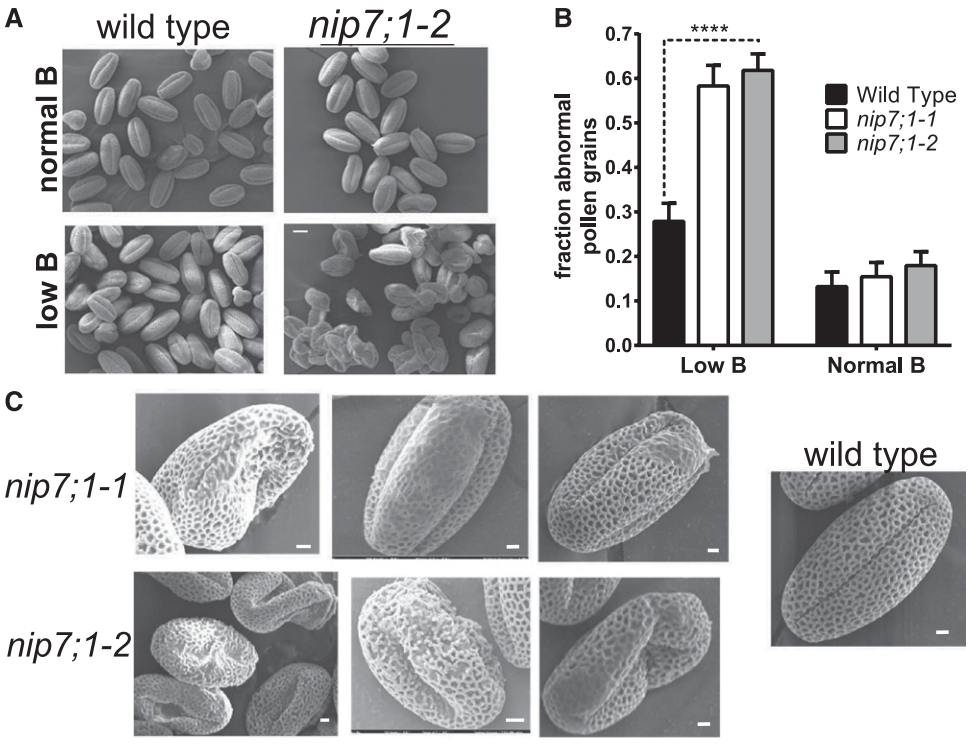

Figure 8. Morphology of wild-type and *nip7;1* pollen. A, SEM comparison of mature pollen grains from wild-type and *nip7;1-2* plants grown under normal (100 µM) and low (0.3 µM) boric acid. Bar = 10 µm. B, Analysis of the fraction of pollen grains exhibiting defective exine patterning or abnormal morphology under normal or low-boric acid conditions. The data represent the analysis of 200 to 300 pollen grains for each treatment, with the error bars representing the SE. ****, $P < 0.0001$ from an unpaired Student's t test of the data. C, SEM images showing representative defects of *nip7;1-1* and *nip7;1-2* pollen grains isolated from plants grown under low-boric acid conditions. For comparison, a wild-type pollen grain obtained under identical conditions (which shows normal morphology) is shown at right. Bars = 2 µm.

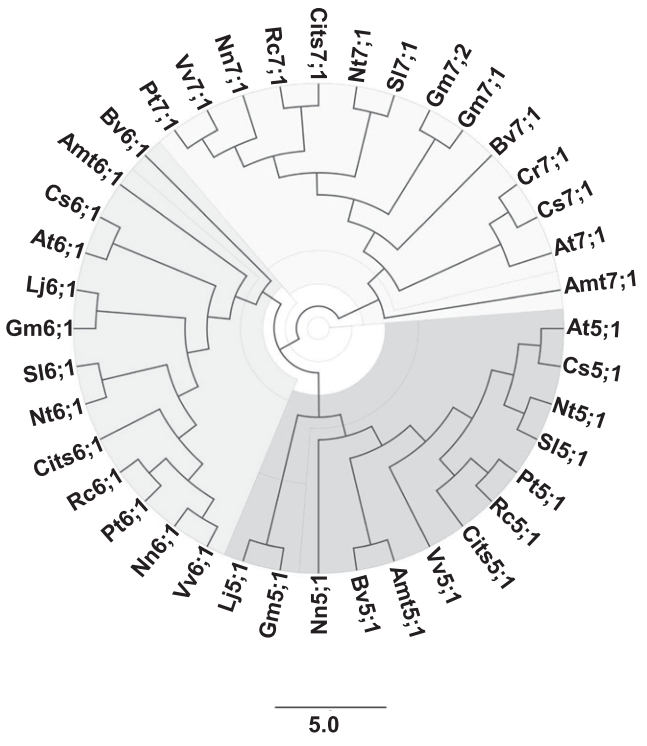

Figure 9. Phylogeny of NIP II proteins in dicots. An unrooted phylogenetic tree is shown for representative NIP5;1, NIP6;1 and NIP7;1 proteins from various dicot lineages, including: Amt, *Amborella trichopoda*; At, *Arabidopsis thaliana*; Bv, *Beta vulgaris*; Cits, *Citrus sinensis*; Cr, *Capsella rubella*; Cs, *Camelina sativa*; Gm, *Glycine max*; Lj, *Lotus japonicus*; Nn, *Nelumbo nucifera*; Nt, *Nicotiana tabacum*; Pt, *Populus trichocarpa*; Rc, *Ricinus communis*; Sl, *Solanum lycopersicum*; Vv, *Vitis vinifera*. Specific gene accession information for each protein is available in Supplemental Table S1. The scale bar represents the length corresponding to five amino acid substitutions per 10 residues.

by the presence of a gating Tyr residue found one α-helical turn away from the ar/R selectivity H2 residue on helix 2 (Li et al., 2011; Fig. 2; Supplemental Table S1). This Tyr in the H2-4 position is unique to the NIP7;1 clade and is invariant in all eudicot lineages (Supplemental Table S1), while the earliest basal dicot species *Amborella trichopoda* possesses a different hydroxylated amino acid, Ser, at this position. Structural modeling and molecular dynamics calculations show that this Tyr adopts either a down orientation, associating with the ar/R Arg, which closes the pore, or an up orientation, facing the extracellular side of the membrane, which results in an open pore (Fig. 2). *X. laevis* oocyte data show that this Tyr residue confers a low intrinsic boric acid permeability of NIP7;1, which suggests that the down/closed state is favored in *X. laevis*. This is supported by the observation that the replacement of Y81 with a smaller residue at position 81 (e.g. the Cys residue in NIP7;1Y81C) opens the channel pore. The fact that NIP7;1Y81C is open in both oocytes and proteoliposomes, whereas NIP7;1 is open only in proteoliposomes, supports the hypothesis that Tyr-81 regulates the wild-type protein and may function as a gating residue.

The biochemical/biophysical parameters that lead to the preferential occupation of an up or down state in these two systems is not clear, but it could be due to differences in the properties of the lipid bilayer that have been shown in other systems to control membrane/protein interaction and packing (Phillips et al., 2009) and aquaporin activity (Tong et al., 2012, 2013). More importantly, the potential regulation of the transport permeability of NIP7;1 in planta remains an open question. Based on extensive study of a wide variety of aquaporins, pore structure and permeability can be regulated at multiple levels, including protein-protein interaction (both with other aquaporin monomers and extrinsic regulatory proteins), pH modulation, and posttranslational modification (Chaumont and Tyerman, 2014; Sachdeva and Singh, 2014; Kreida and Törnroth-Horsefield, 2015; Maurel et al., 2015; Roche and Törnroth-Horsefield, 2017). How these parameters might influence NIP7;1 activity needs further investigation.

NIP7;1 Is Induced during the Pollen Microsporogenesis Stage of Anther Development and Is Expressed Predominantly in Tapetal Cells

NIP7;1 is expressed predominantly in the anthers of developing flowers in a narrow developmental window, appearing at floral stage 8, peaking at stage 9, persisting through stage 10 and early stage 11, and disappearing by stage 12. From a developmental perspective, pollen microsporocytes enter and complete meiosis to form a tetrad of microspores surrounded by a callose cell wall during flower stage 9 (Sanders et al., 1999). In stage 10 flowers, individual pollen microspores are released from the tetrad and generation of the exine pollen cell wall is initiated (Sanders et al., 1999; Liu and Fan, 2013). At stages 11 and 12, pollen mitotic divisions occur, pollen cell wall biosynthesis is completed, and mature tricellular pollen grains are generated (Sanders et al., 1999; Liu and Fan, 2013).

Investigation of *NIP7;1* ortholog genes in other dicotyledonous species supports the conclusion that they are expressed preferentially in reproductive tissues compared with vegetative tissues (Zou et al., 2015; Li et al., 2016; Supplemental Fig. S6). Furthermore, in cases where data are available, it also is clear that *NIP7;1* is specific for male-specific flowers or tissues at early developmental stages associated with pollen meiosis and microsporogenesis (Li et al., 2016; Supplemental Fig. S6). Overall, these data support a conserved role for NIP7;1 in male gametogenesis and pollen development that emerged during dicot evolution. Unlike the root *NIP5;1* boric acid permease, which is induced by low environmental B (Takano et al., 2006), expression analysis of *NIP7;1* in flowers shows only a minor fluctuation (40% increase) upon reduction of medium boric acid from 100 to 1 μM (Supplemental Fig. S7). Thus, *NIP7;1* expression may be regulated principally as part

of the flower development program rather than in response to environmental B.

Cellular localization studies with *NIP7;1pro*::*GUS* transgenic plants showed the accumulation of GUS signal in both developing microspores and tapetal cells. This is consistent with previous observations utilizing in situ localization with *NIP7;1*-specific probes, which detected the *NIP7;1* transcript in developing pollen grains (Li et al., 2011). However, in contrast to the GUS and transcript localization data, cellular localization of NIP7;1 using two native promoter-translational YFP fusions shows that, in developing Arabidopsis flowers, the protein is detected only within the tapetum, the innermost cell layer surrounding the anther locule. The reason for this apparent discrepancy in mRNA expression and protein accumulation is not clear. While it is possible that NIP7;1 protein is expressed at a low level in microspores that evaded detection, the data show that the protein is expressed preferentially at high levels in the tapetum compared with other floral tissues. Thus, it is proposed that it plays a predominant role in this tissue (Fig. 4C).

The tapetum plays a fundamental developmental role during floral stages 9 and 10 by providing metabolites, nutrients, and other components to the developing pollen grain (Liu and Fan, 2013). At stage 11, pollen mitotic divisions occur and the degeneration of the tapetum by programmed cell death occurs (Sanders et al., 1999; Liu and Fan, 2013), releasing the contents of tapetal cells, which become associated with the outer coat of mature pollen grains (Hsieh and Huang, 2007). The critical role of the tapetum in pollen development is underscored by the observations that defects in tapetal genes often are associated with defective pollen cell wall formation and male sterility (Liu and Fan, 2013; Shi et al., 2015).

The NIP II protein NIP5;1 shows strong and polarized localization to the plasma membrane, with the coordinated membrane position of BOR transporters facilitating a directional flow of boric acid/borate to tissues of need (Takano et al., 2007, 2010; Wang et al., 2017). Polar plasma membrane localization of NIP5;1 is mediated by the phosphorylation of conserved Thr residues within the N-terminal domain (Wang et al., 2017). This motif is conserved in NIP6;1 proteins, which also show polarized plasma membrane localization, whereas NIP7;1, which lacks this motif, accumulated inside the cell when expressed heterologously under the control of the *NIP5;1* promoter in Arabidopsis roots (Wang et al., 2017). In this study, the expression of NIP7;1-GFP driven by its native promoter was assessed, and it was observed that the protein is localized to the plasma membrane of tapetal cells but also was detected within cytosolic structures as well. Both plant and animal aquaporins and aquaporin-like proteins show dynamic properties and trafficking to different subcellular localizations in response to changing physiological conditions (for review, see Takano et al., 2017), and this also may be a property of NIP7;1. Nevertheless, the plasma membrane localization of NIP7;1, together with the B-dependent phenotype of *nip7;1* mutants (see below), argue for a role for NIP7;1 in mediating the uptake of boric acid into the tapetum necessary for pollen development.

NIP7;1 as a Tapetal Boric Acid Channel during Pollen Development

In this study, it was found that loss of function of *NIP7;1* results in developmental and pollen cell wall phenotypes that are manifested under limiting conditions of boric acid. Under B limitation, *nip7;1* pollen grains show reduced viability, irregular morphology, an increased incidence of grains clumping into aggregates, and poor exine formation, with a compromise of the typical reticulate outer cell wall and breaks in the exine structure. TEM examination of the ultrastructure of *nip7;1* pollen under B limitation shows that, while some elements of the pollen cell wall are present (e.g. intine and nexine), the outer exine layer is reduced or lacking, with poor formation of the bacula and tecta structures that form the ornate reticular pollen wall.

The defects observed in pollen formation in the *nip7;1* plants are consistent with the B nutritional defects in reproductive growth observed with several plant species. For example, anther development and pollen microsporogenesis are particularly sensitive to B limitation, and male sterility is a common outcome of limiting B (Rawson, 1996; Dell and Huang, 1997; Huang et al., 2000). Investigation of B and pollen development in wheat (*Triticum* spp.) showed that the most sensitive stage of microsporogenesis to B deficiency was the phase between the premeiotic interphase through meiosis to the late tetrad stage (Rawson, 1996; Huang et al., 2000). This phase would correspond to flower developmental stages 9 and 10 in Arabidopsis, the flower stages with maximal *NIP7;1* expression. Under B-deficient conditions, defects in pollen morphology, including empty or misshapen pollen grains (Dell and Huang, 1997) and poorly developed exine cell walls (Smith et al., 1997), have been observed. Finally, global disruption of B homeostasis by mutations of borate/boric acid transporters and channels also results in sterile phenotypes (Chatterjee et al., 2014; Durbak et al., 2014; Zhang et al., 2017) or defective pollen function (Tanaka et al., 2013; Alva et al., 2015), underscoring the importance of directed B transport in reproductive development. Interestingly, in the case of maize (*Zea mays*), the *tassel-less* mutant was found to be the result of the loss of function of a boric acid transport NIP II protein that is expressed in male inflorescences and roots (Durbak et al., 2014). Since NIP7;1 is a dicot-specific protein that is lacking in monocot lineages, it may play an analogous role to the *tassel-less* maize NIP in providing boric acid for reproductive development.

Previous work (Isayenkov and Maathuis, 2008; Lindsay and Maathuis, 2016) has shown that *nip7;1* mutants exhibit higher tolerance to arsenate or arsenite, and a role has been proposed for NIP7;1 in the partitioning

of arsenic (As) metalloids between the roots and shoots (Lindsay and Maathuis, 2016). In this regard, similar to other NIP proteins (Pommerrenig et al., 2015), NIP7;1 may function as an $As(OH)_3$ permease in response to the soil accumulation of this toxic metalloid. Based on these observations, and the observation that NIP7;1 is expressed at a low level in roots, it is possible that the developmental defect observed in *nip7;1* plants could be the result of low uptake of B in the roots as well as defects in partitioning within the anther tissues. However, two observations in this study suggest that the observed reproductive defects may be associated preferentially with its function in the flower: (1) *nip7;1* T-DNA mutants (Supplemental Fig. S4) did not appear to exhibit the drastic B developmental phenotypes in vegetative tissues readily apparent in mutants of *nip5;1* (Takano et al., 2006) and *nip6;1* (Tanaka et al., 2008); and (2) analysis of the B content of the roots and shoots under low-B conditions by inductively coupled plasma mass spectrometry (ICP-MS; Supplemental Fig. S8) showed that the B content was not significantly different between wild-type and *nip7;1* mutant plants. While previous work provides a potential role of vegetative NIP7;1 in As distribution under growth in As-containing medium (Lindsay and Maathuis, 2016), and while we cannot exclude that NIP7;1 might play a minor role in boric acid permeability within selected root tissues, our findings indicate that the pollen developmental phenotypes observed here likely are associated with its function within tapetal cells.

Genetic defects that lead to poor exine formation are associated with male-sterile phenotypes. Thus, the exine defects in *nip7;1* pollen may be a principal feature that accounts for the increased sterility observed under limiting B. To understand the potential role of *nip7;1* in exine development, one must consider the developmental profile of pollen cell wall formation and the role of the tapetum. Pollen cell wall formation is a spatially and temporally regulated process that involves the synthesis, secretion, and assembly of various components, including callose, a microfibrilar primexine template, the elaborate reticulate outer exine wall, and the inner pectocellulosic intine (for review, see Blackmore et al., 2007; Ariizumi and Toriyama, 2011; Liu and Fan, 2013; Shi et al., 2015). During floral stage 9, meiosis and the generation of microspore tetrads is associated with the synthesis of the microfibrilar primexine cell wall layer on the developing microspores, presumably from the secretion of pectocellulosic precursors from the tapetum (Aouali et al., 2001; Ariizumi and Toriyama, 2011). The primexine serves as a template and scaffold for the deposition of sporopollenin, a polymer of long-chain fatty acids and phenylpropanoids that is synthesized and secreted by the tapetum (Liu and Fan, 2013). This results in the formation of preexine structures known as probacula that serve as assembly sites for exine precursors on the primexine substratum. Genetic defects in primexine formation are associated with poor anchoring of sporopollenin substrates, disruption in exine patterning, and sterility (Suzuki et al., 2008, 2017; Hu et al., 2014; for review, see Ariizumi and Toriyama, 2011). During floral stage 10, β-1,3-glucanases released by the tapetum cleave tetrads into single pollen microspores, sporopollenin deposition and exine formation continue to proceed, and the synthesis of the pectocellulosic intine layer is initiated in the developing microspore. During floral stages 11 and 12, pollen mitotic cell divisions occur, and the tapetum undergoes programmed cell death, releasing cellular contents into the anther locule that are deposited on mature pollen grains, forming the hydrophobic pollen coat or tryphine layer. This layer plays an essential role in the attachment of the pollen to the stigma, proper hydration, and pollen germination during fertilization (Hsieh and Huang, 2004; Shi and Yang, 2010).

The importance of B and pectic RG-II in pollen development and tapetum function is underscored by the findings of Iwai et al. (2006). By using tobacco (*Nicotiana plumbaginifolia*), they showed that the pectin glucuronsyl transferase gene *NpGUT1*, which is essential for the formation of B cross-linked RG-II, is highly expressed in the tapetum and that RNA interference knockdown of *NpGUT1* expression in flower buds results in male sterility. The expression of *NIP7;1* during stages 9 and 10 suggests that it functions as a tapetal boric acid channel necessary for pollen cell wall development by promoting boric acid uptake, presumably for the synthesis of pectins, which are secreted from the tapetum and are incorporated into the pectocellulosic primexine template on developing microspores during these developmental stages (Aouali et al., 2001). The poor formation of the outer exine wall in *nip7;1* mutants suggests that alterations in primexine formation may affect the early stages of exine patterning. Based on the transporter-channel collaborative hypothesis (Takano et al., 2008) for B homeostasis, it will be interesting to investigate the potential transporters of the BOR family that may be coexpressed with NIP7;1 during this critical stage of pollen development and that coordinate B homeostasis in developing anthers.

MATERIALS AND METHODS

Plant Materials and Growth

Arabidopsis (*Arabidopsis thaliana*) plants used in this study are in the Columbia-0 ecotype background. Seed sterilization, stratification, and growth under standard long-day conditions were done as described previously (Choi and Roberts, 2007). The T-DNA mutants *nip7;1-1* (SALK_042590) and *nip7;1-2* (SALK_057023) were identified from the collection of the Salk Institute Genomic Analysis Laboratory, and the corresponding seeds were obtained from the Arabidopsis Biological Resource Center. The T-DNA insertion site was verified and the genotype of *nip7;1* mutant plants was determined by using the Salk PCR genotyping protocol (http://signal.salk.edu/tdnaprimers.2.html). Genomic DNA was extracted from small rosette leaves as described by (Zhou et al., 2011), and PCR was performed with primer sets that flank the proposed site of the T-DNA insertion for each mutant as well as with a primer for the T-DNA left border (primer sequences are shown in Supplemental Table S2). PCR products were cloned into the pCR2.1-TOPO vector (Invitrogen), and the site of insertion was verified by Sanger sequencing performed at the University of Tennessee Genomic Core Facility. Homozygous *nip7;1* lines were used for

all analyses. To verify the loss of expression in T-DNA mutants, comparative expression of the *NIP7;1* transcript in 6-week-old inflorescences of wild-type and *nip7;1* plants was tested by isolation of mRNA as described by Choi and Roberts (2007) followed by end-point RT-PCR analysis (Supplemental Fig. S2) with *NIP7;1*-specific primers (Supplemental Table S2). *UBQ10* was used as the internal reference gene.

To determine the effects of limiting B on growth and development, wild-type and *nip7;1* plants were grown in defined MGRL medium (Fujiwara et al., 1992) supplemented with different boric acid concentrations. Arabidopsis seedlings were germinated and grown in medium with 60 μM boric acid for 3 weeks until the 10th rosette leaf was greater than 1 mm. The plants then were transferred to liquid MRGL medium supplemented with either 100 μM (high B) or 0.3 μM (low B) boric acid and were grown hydroponically with aeration under long-day conditions (16-h-light/8-h-dark cycle) at 22°C through flowering and seed set. During this growth period, the medium was changed every 4 d.

B analysis of tissues from 6-week-old Arabidopsis plants under different boric acid growth conditions was done by the nutrient analysis technique of Barickman et al. (2013) with slight modifications. Briefly, samples were dried for 48 h in a forced-air oven (Fisher Scientific) at 45°C. Samples were ground to less than 20 mesh. A 0.1-g sample was combined with 5 mL of 70% (v/v) HNO_3 and digested in a microwave digestion unit (Ethos; Milestone). Nutrient analysis was conducted using ICP-MS (Agilent Technologies). The ICP-MS system was equipped with an octapole collision/reaction cell, Agilent 7500 ICP-MS ChemStation software, a Micromist nebulizer (Agilent Technologies), a water-cooled quartz spray chamber, and a CETAC (ASX-510) autosampler. The instrument was optimized daily in terms of sensitivity (lithium [Li], yttrium [Y], and thallium [Tl]), level of oxide (cerium [Ce]), and doubly charged ion (Ce) using a tuning solution containing 10 μg L^{-1} Li, Y, Tl, Ce, and cobalt in a 2% HNO_3/0.5% HCl (v/v) matrix. Tissue nutrient concentrations are expressed on a dry weight basis.

In vitro pollen germination was performed with harvested wild-type and mutant pollen utilizing the solid pollen germination medium formulation and method of Bou Daher et al. (2009). Five to 10 flowers that had just opened (stage 13 flowers) were collected and were brushed onto solid medium to release the pollen grains. Pollen grains were germinated by incubation for 16 h at 22°C. Images of germinated pollen were collected using a dissecting microscope and were scored for germination frequency. Successful germination was taken as the presence of emerged pollen tubes that extend longer than the pollen grain diameter. Over 250 pollen grains were scored for each sample.

Recombineering lines containing translational fusions of NIP7;1 with three in-frame C-terminal copies of YFP were generated by the approach of Zhou et al. (2011). JAtY clone information and primers for *NIP7;1* (JAtY68K23) were obtained from resources available at https://alonsostepanova.wordpress.ncsu.edu/welcome/research-interests/recombineering/. JAtY68K23 was purchased from the Genome Analysis Center. The *Escherichia coli* recombineering strain SW105 was purchased from Frederick National Laboratory for Cancer Research, and the recombineering cassette with 3xYpet was generously provided by Dr. Jose Alonso (University of North Carolina). The 3xYpet cassette was fused to the C-terminal coding region of *NIP7;1* by PCR using Rec F and Rec R primers (Supplemental Table S2). The correct constructs were verified by automated DNA sequencing. The 3xYpet-tagged JAtY68K23 clone was transformed to *Agrobacterium tumefaciens* GV3101, and transgenic recombineering strains were generated as described (Zhou et al., 2011). The transformants were selected on Murashige and Skoog medium supplemented with 20 μg mL^{-1} glufosinate ammonium and 300 μg mL^{-1} timentin. The recombineering lines containing the *NIP7;1-3YFP* construct were genotypically confirmed by PCR of genomic DNA using NIP7;1-specific primers (71F and 71R) and 3xYpet-specific primers (3xYpet; Supplemental Table S2).

The *proNIP7;1:NIP7;1-GFP* construct was generated as follows. The vector fragment with monomeric GFP (mGFP) was PCR amplified with primers (pGWB504m L and pGWB504m R) using the pGWB504m vector (Segami et al., 2014) as a template. A genomic fragment containing the *NIP7;1* promoter region and coding sequence was PCR amplified with primers (Nos. 1989 and 2002) using Columbia-0 genomic DNA as a template. These fragments were fused using the In-Fusion HD Cloning Kit (Takara Clontech). A linker encoding five amino acids (GGGGS) was inserted between *NIP7;1* and *mGFP*. The sequence for the coding region was confirmed by sequencing. The construct was introduced into *A. tumefaciens* GV3101::pMP90 strains and used for the transformation of *nip7;1-2* mutant plants by the *A. tumefaciens*-mediated floral dip method (Clough and Bent, 1998). The transformants were selected on MGRL medium (Takano et al., 2005) supplemented with 30 μM boric acid, 1% (w/v) Suc, 20 μg mL^{-1} hygromycin, and 250 μg mL^{-1} claphoran.

Microscopy Techniques

For TEM examination, flower tissues were fixed with 4% (w/v) paraformaldehyde overnight at 4°C and then with 1% (w/v) osmium tetroxide in 50 mM sodium phosphate and 0.21 M Suc for 2 h at 4°C. Fixed sections were embedded in Spurr's resin as described (Choi and Roberts, 2007), and thin sections (100 nm) were obtained with a Leica EMFC7 ultramicrotome. Sections were mounted on copper grids and were stained with 2% (w/v) aqueous uranyl acetate for 20 min, followed by staining with Reynolds' lead citrate (Reynolds, 1963) for 5 min. The samples were observed using a Zeiss Libra 200 HT FE MC transmission electron microscope. For SEM examination, fresh pollen grains from wild-type or mutant flowers were attached to an adhesive carbon tape on the top surface of a SEM sample holder. The specimens were coated with gold by using an SPI sputter coater (SPI Suppliers) and then observed with a Zeiss Auriga scanning electron microscope at 5 kV. All electron microscopy measurements and procedures were performed at the Advanced Microscopy and Imaging Center (AMIC) at the University of Tennessee in Knoxville.

Live tissue confocal fluorescence microscopy of *NIP7;1-3YFP* recombineering lines was done using the Leica SP8 White Light Laser Confocal System at the Advanced Microscopy and Imaging Center at the University of Tennessee. For live cell imaging, intact anthers of various flower stages were dissected, and confocal microscopic examination was conducted with a white light laser of 15% intensity, the pinhole set to 1 Airy Unit, the gain set to 100%, gating set at 0.3 to 6, with the fluorifer disc setting at NF514. The YFP signal was visualized with an excitation wavelength of 514 nm, and emission was detected at 525 to 570 nm. To visualize plastids, the emission was set at 650 to 720 nm. Images were captured using the Leica Application Suite X software provided with Leica Sp8 inbuilt software using 10×, 40×, or 63× oil-immersion objectives. Intact flowers were incubated with 4% (w/v) paraformaldehyde in phosphate-buffered saline (10 mM sodium phosphate, pH 7.2, and 0.15 M NaCl) at 4°C for 16 h, washed with phosphate-buffered saline, embedded with London White Resin as described (Bell et al., 2013), and sectioned (1–2 μm) with an ultramicrotome prior to confocal microscopy.

Live tissue confocal fluorescence microscopy of *NIP7;1pro::NIP7;1-GFP* plants was done using the Leica SP8 equipped with hybrid detectors and a 40× water-immersed lens at Osaka Prefecture University. The T2 plants were grown for 5 weeks under standard conditions on rockwool and vermiculite. To visualize GFP, samples were excited by a 488-nm diode laser, and emission was detected at 500 to 530 nm by a hybrid detector. To visualize plastids, samples were excited by a 488-nm diode laser, and emission was detected at 650 to 700 nm . The pinhole was set to 1 Airy Unit.

GUS staining and visualization were conducted on Arabidopsis inflorescences of 6-week-old transgenic *NIP7;1pro::GUS* reporter plants (Li et al., 2011) by using the procedure of Choi and Roberts (2007). *GUS* reporter plants driven by the *NIP7;1* promoter were generated as described (Li et al., 2011). The results of a single transformed line are shown in this study. GUS-stained tissues were observed and imaged using a Nikon ECLIPSE E600 microscope and QCapture 2.60 software (QImaging). For cellular localization determination, GUS-stained tissues were dehydrated using 100% ethanol for 30 min followed by two propylene oxide treatments for 25 min each. The tissue was then infiltrated with Spurr's epoxy resin (Electron Microscopy Sciences) and propylene oxide mixture (1:4, 1:2, 1:1, 2:1, and 4:1) volume ratio for at least 8 h each followed by 100% Spurr's resin. Samples embedded in Spurr's resin were polymerized at 60°C overnight. Sections (10 μm thick) were obtained by using a Leica (Reichert) OMU3 ultramicrotome, and GUS staining was observed using a Nikon Eclipse E600 microscope equipped with QCapture 2.6 software (QImaging).

Pollen viability was determined by staining with a vital dye utilizing the procedure of Dupl'áková et al. (2016). Pollen from freshly opened flowers (stage 13) were collected and incubated in fluorescein diacetate (20 μM) in 10% (w/v) sucrose for 10 min in the dark. Pollen viability, judged by the fluorescent signal resulting from the uptake and hydrolysis of the diacetate derivative to release of fluorescein, was determined by fluorescence microscopy with a Leica DM 60000B epifluorescence microscope with the excitation wavelength set to 488 nm and the emission filter set between 515 and 550 nm.

Recombinant NIP7;1 and NIP7;1Y81C Purification and Reconstitution

NIP7;1 and NIP7;1Y81C coding sequences were codon optimized for *Pichia pastoris* by using the OptimumGene codon optimization analysis system (GenScript), and synthetic genes were produced and subcloned as N-terminal His-tagged fusions into the *Bam*HI and *Not*I restriction sites of the pPIC3.5K

expression vector (Life Technologies). Expression constructs were transformed into *P. pastoris* as described in the EasySelect *Pichia* Expression handbook (Life Technologies). Clones with multiple inserts were identified by selection on medium with 1.75 mg mL^{-1} geneticin sulfate (G418), and protein expression levels in various transformants were determined by a western-blot assay by the protocol of Hwang et al. (2010). Clones exhibiting high expression levels were cultured for protein expression on IsoYeast medium (Sigma) by the procedure of Hwang et al. (2010) with modifications. After methanol induction, cells were collected by centrifugation and lysed in a French Pressure Cell in 20 mM Tris-HCl, pH 8, 100 mM NaCl, 1 μg mL^{-1} leupeptin, 1 μg mL^{-1} pepstatin A, and 0.5 mM phenylmethanesulfonyl fluoride. The extract was centrifuged at 7,000*g* for 45 min at 4°C, followed by centrifugation of the supernatant fraction at 200,000*g* for 2 h at 4°C to collect membranes. The membrane pellet was suspended in 20 mM Tris-HCl, pH 8, 100 mM NaCl, 10% (v/v) glycerol, 20 mM imidazole, and 2% (w/v) *n*-dodecyl-*β*-D-maltopyranoside (DDM; Anatrace) and was mixed gently for 16 h at 4°C to solubilize the NIP7;1 proteins. The mixture was centrifuged at 12,000*g* for 20 min, and the supernatant fraction was applied to Ni^{2+}-NTA resin (1-mL packed volume; Qiagen). The resin was washed with 100 volumes of 20 mM Tris-HCl, pH 8, 300 mM NaCl, 35 mM imidazole, and 0.03% (w/v) DDM and was eluted with 20 mM Tris-HCl, pH 8, 100 mM NaCl, 500 mM imidazole, and 0.02% (w/v) DDM. The eluent was chromatographed on a Superdex 200 10/200 GL column (GE Healthcare) in 20 mM Tris-HCl, pH 8, 100 mM NaCl, and 0.02% (w/v) DDM. Fractions containing pure, unaggregated protein were collected, and the purity was verified by SDS-PAGE as described (Hwang et al., 2010). The final pooled protein fractions were concentrated to 1 mg mL^{-1} using a Vivaspin sample concentrator with a 50-kD cutoff (GE Healthcare).

For the generation of proteoliposomes, 5 mg of *E. coli* total lipids (Avanti Polar Lipids) was suspended by bath sonication in 1 mL of 50 mM HEPES NaOH, pH 7.4, 50 mM NaCl, 10 mM carboxyfluorescein (CF), and 200 mM boric acid and extruded 40 times through a mini extruder (Avanti Polar Lipids) to produce small unilamellar vesicles. Reconstitution of NIP7;1 into liposomes was done by the general method of Knol et al. (1998). Briefly, 3.25 mg of DDM (detergent-to-lipid ratio of 0.65, w/w) was combined with the liposome suspension and incubated for 1 h at 4°C. NIP7;1 or NIP7;1Y81C (lipid-to-protein ratio of 80:1, w/w) was added, and the incubation was continued for an additional 1 h at 4°C. Excess DDM was removed by detergent-absorbing polystyrene beads (Bio-Beads SM2 Adsorbent; Bio-Rad Laboratories) by the method of Rigaud and Lévy (2003). Control liposomes were formed by an identical procedure in the absence of NIP7;1 protein. External CF dye was removed by chromatography on a PD-10 desalting column (GE Healthcare) in 10 mM HEPES NaOH, pH 7.4, 50 mM NaCl, and 200 mM boric acid. The incorporation of NIP7;1 protein into the final proteoliposomes was verified by SDS-PAGE and western blot.

Permeability Measurements

Solute permeability measurements of CF-loaded proteoliposomes were performed by stopped-flow fluorimetry as described (Rivers et al., 1997; Dean et al., 1999). The liposomes were loaded with 10 mM CF, a volume-sensitive dye, and 200 mM of the test solute (in this case, boric acid). Liposomes were mixed abruptly in an equal volume of isoosmotic medium with nonpermeant solutes (10 mM HEPES NaOH, 150 mM NaCl, 350 mOsm kg^{-1}). As boric acid fluxes from the interior of the liposomes, water osmotically follows and the rate of liposome vesicle shrinkage (reported as a decrease in fluorescence due to CF quenching) is dependent on the rate of boric acid efflux (the rationale is shown in Supplemental Fig. S1). Fluorescence measurements were performed using an Applied Photophysics model SX stopped-flow spectrofluorimeter. As described previously (Dean et al., 1999), fluorescence traces of 10 to 16 injections were collected, analyzed, and averaged to reduce spectral noise by using Pro-Data software (Applied Photophysics). For the permeability measurements shown in this study, the data from each injection deviated by less than a 2% coefficient of variance from the mean for each data set. By using Prism software (version 6; GraphPad), the fluorescence data in the average time trace were well fit with a single exponential function, $F_{(t)} = (a)*e^{-bt} + c$ (R^2 = 0.993–0.999 for boric acid and glycerol; R^2 = 0.956–0.975 for water), where $F_{(t)}$ is the relative fluorescence intensity at time t, a is the amplitude of the curve, b is the rate constant for the exponential decay, and c is the end point of the curve. The rate constant from this fit was used to calculate P_B (measured in cm s^{-1}) by using the differential equations described by Mathai and Zeidel (2007), which were modified according to the parameters in this study:

$$\frac{dV_{rel}}{dt} = (P_B)\left\{\frac{S_A/V}{V_0}\right\}(1/3500)\left\{\frac{500}{V_{rel}} - 600\right\} \quad (1)$$

where S_A/V is the surface area-to-volume ratio, V_0 is the initial volume, V_{rel} is the relative volume of the liposome vesicle, and dV_{rel}/dt is the change of vesicular volume per unit of time. The diameters of proteoliposomes and liposomes were determined by dynamic light scattering by the method of Drin et al. (2008) using a Dynapro NanoStar instrument (Wyatt Technology). The S_A/V was calculated from the following ratio:

$$\frac{4\pi r^2}{\left\{\frac{4\pi r^3}{3}\right\}} = \frac{3}{r} \quad (2)$$

where *r* is the vesicular radius. The internal vesicular volumes of liposome preparations were determined fluorimetrically as described (Rivers et al., 1997). The system of differential equations was solved numerically by using the Mathematica 9 software package (Wolfram). The osmotic water permeability of liposomes and proteoliposomes was determined as described (Dean et al., 1999). Boric acid permeability measurements in *Xenopus laevis* oocytes were done by using the swelling assay of Wallace and Roberts (2005) with the parameters of Li et al. (2011).

Bioinformatic and Modeling Methods

The AQP4 tetramer structure (pdb 3GD8) was used as the structural template for homology modeling using the Molecular Operating Environment (MOE 2009.10) software. The NIP7;1 sequence was aligned with the four chains of AQP4, homology modeling was done in MOE, and biological assemble (BIOMT) transformation was performed in order to generate the homotetramer NIP7;1 model using MOE. The homology model was energy minimized using the CHARMM27 force field and distance-dependent dielectric down to an energy gradient of 10 to 5 kcal mol^{-1} $Å^{-2}$. All *α*-carbons were fixed during the energy minimization, to prevent swelling of the transmembrane region of the protein. Molecular dynamics were run at a temperature of 310 K for 5 ns, using a 1-ps integration time step in the isothermal-isobaric thermodynamic ensemble. Selected down versus up conformations were used for model building, with glycerol docked into the open (up) conformation based on the structure of the glycerol facilitator/glycerol complex (pdb 1FX8).

Selected orthologs of NIP5;1, NIP6;1, and NIP7;1 families from various dicots were identified by a BLASTP search using the Arabidopsis NIP5;1, NIP6;1, and NIP7;1 amino acid sequences as the search query. Gene accession information for all proteins is available in Supplemental Table S1. Multiple sequence alignments were generated by using the ClustalW algorithm in the slow-accurate mode in the MegAlign13 program in the DNA Laserstar 13 Package. Phylogenetic trees were generated in MegAlign13 and were exported as PAUP*4 files to FigTree 1.4.2 (http://tree.bio.ed.ac.uk/) to generate phylogram figures.

Accession Numbers

The accession numbers of the genes mentioned in this study are as follows: *NIP5;1* (At4g10380), *NIP6;1* (At1g80760), and *NIP7;1* (At3g06100). Others accession numbers are documented in Supplemental Table S1.

Supplemental Data

The following supplemental materials are available.

Supplemental Figure S1. Determination of permeability coefficients of proteoliposomes for test solutes.

Supplemental Figure S2. GUS expression in *AtNIP7;1pro*::*GUS* transgenic plants.

Supplemental Figure S3. Map of *nip7;1* T-DNA insertion mutants and RT-PCR of *NIP7;1* expression.

Supplemental Figure S4. Comparison of *nip7;1* mutant plants grown hydroponically under low and normal boric acid.

Supplemental Figure S5. Ultrastructure of the cell wall of wild-type and *nip7;1* mutant pollen from flowers grown under low-boric acid conditions.

Supplemental Figure S6. *NIP7;1* transcript expression from various dicots.

Supplemental Figure S7. *NIP7;1* transcript expression in response to different boric acid concentrations.

Supplemental Figure S8. B content of wild-type, *nip7;1-1*, and *nip7;1-2* plants grown under high- and low-boric acid conditions.

Supplemental Table S1. NIP II proteins of dicots.

Supplemental Table S2. Oligonucleotide primers used in this study.

ACKNOWLEDGMENTS

We thank Dr. John Dunlap (Advanced Microscopy and Imaging Center, University of Tennessee) for microscopy technical support, Dr. Sally Ellingson (University of Kansas Division of Biomedical Informatics) for assistance in permeability measurements and calculation, and Jennifer Wheeler of the University of Tennessee Institute of Agriculture for technical assistance for the ICP-MS measurements. We acknowledge and thank Dr. Jose Alonso and Dr. Anna Stepanova (University of North Carolina) for helping to construct the recombineering-aided tagging system. We also express our appreciation to Shota Hozuki (Hokkaido University) and Keishi Ohshima (Osaka Prefecture University) for the generation of *NIP7;1pro::NIP7:1-GFP* plants and to Dr. Shoji Segami (Nagoya University) for providing a vector containing monomeric GFP.

Received August 3, 2018; accepted September 3, 2018; published September 28, 2018.

LITERATURE CITED

Abascal F, Irisarri I, Zardoya R (2014) Diversity and evolution of membrane intrinsic proteins. Biochim Biophys Acta **1840**: 1468–1481

Alva O, Roa-Roco RN, Pérez-Díaz R, Yáñez M, Tapia J, Moreno Y, Ruiz-Lara S, González E (2015) Pollen morphology and boron concentration in floral tissues as factors triggering natural and GA-induced parthenocarpic fruit development in grapevine. PLoS ONE **10**: e0139503

Aouali N, Laporte P, Clément C (2001) Pectin secretion and distribution in the anther during pollen development in Lilium. Planta **213**: 71–79

Ariizumi T, Toriyama K (2011) Genetic regulation of sporopollenin synthesis and pollen exine development. Annu Rev Plant Biol **62**: 437–460

Barickman TC, Kopsell DA, Sams CE (2013) Selenium influences glucosinolate and isothiocyanates and increases sulfur uptake in Arabidopsis thaliana and rapid-cycling Brassica oleracea. J Agric Food Chem **61**: 202–209

Bell K, Mitchell S, Paultre D, Posch M, Oparka K (2013) Correlative imaging of fluorescent proteins in resin-embedded plant material. Plant Physiol **161**: 1595–1603

Bienert MD, Bienert GP (2017) Plant aquaporins and metalloids. *In* **F Chaumont, SD Tyerman**, eds, Plant Aquaporins: From Transport to Signaling. Springer International Publishing, Cham, Switzerland, pp 297–332

Blackmore S, Wortley AH, Skvarla JJ, Rowley JR (2007) Pollen wall development in flowering plants. New Phytol **174**: 483–498

Blevins DG, Lukaszewski KM (1998) Boron in plant structure and function. Annu Rev Plant Physiol Plant Mol Biol **49**: 481–500

Bou Daher F, Chebli Y, Geitmann A (2009) Optimization of conditions for germination of cold-stored Arabidopsis thaliana pollen. Plant Cell Rep **28**: 347–357

Camacho-Cristóbal JJ, Rexach J, González-Fontes A (2008) Boron in plants: deficiency and toxicity. J Integr Plant Biol **50**: 1247–1255

Chatterjee M, Tabi Z, Galli M, Malcomber S, Buck A, Muszynski M, Gallavotti A (2014) The boron efflux transporter ROTTEN EAR is required for maize inflorescence development and fertility. Plant Cell **26**: 2962–2977

Chaumont F, Tyerman SD (2014) Aquaporins: highly regulated channels controlling plant water relations. Plant Physiol **164**: 1600–1618

Choi WG, Roberts DM (2007) Arabidopsis NIP2;1, a major intrinsic protein transporter of lactic acid induced by anoxic stress. J Biol Chem **282**: 24209–24218

Clough SJ, Bent AF (1998) Floral dip: a simplified method for Agrobacterium-mediated transformation of Arabidopsis thaliana. Plant J **16**: 735–743

Danielson JA, Johanson U (2010) Phylogeny of major intrinsic proteins. Adv Exp Med Biol **679**: 19–31

Dean RM, Rivers RL, Zeidel ML, Roberts DM (1999) Purification and functional reconstitution of soybean nodulin **26**: an aquaporin with water and glycerol transport properties. Biochemistry **38**: 347–353

Dell B, Huang LB (1997) Physiological response of plants to low boron. Plant Soil **193**: 103–120

Dell B, Huang L, Bell RW (2002) Boron in plant reproduction.. *In* **H Goldbach, B Rerkasem, MA Wimmer, PH Brown, M Thellier, RW Bell**, eds, Boron in Plant and Animal Nutrition. Springer US, New York, pp 103–117

Drin G, Morello V, Casella JF, Gounon P, Antonny B (2008) Asymmetric tethering of flat and curved lipid membranes by a golgin. Science **320**: 670–673

Dupl'áková N, Dobrev PI, Reňák D, Honys D (2016) Rapid separation of Arabidopsis male gametophyte developmental stages using a Percoll gradient. Nat Protoc **11**: 1817–1832

Durbak AR, Phillips KA, Pike S, O'Neill MA, Mares J, Gallavotti A, Malcomber ST, Gassmann W, McSteen P (2014) Transport of boron by the tassel-less1 aquaporin is critical for vegetative and reproductive development in maize. Plant Cell **26**: 2978–2995

Fortin MG, Morrison NA, Verma DP (1987) Nodulin-26, a peribacteroid membrane nodulin is expressed independently of the development of the peribacteroid compartment. Nucleic Acids Res **15**: 813–824

Fujiwara T, Hirai MY, Chino M, Komeda Y, Naito S (1992) Effects of sulfur nutrition on expression of the soybean seed storage protein genes in transgenic petunia. Plant Physiol **99**: 263–268

Goldbach HE, Huang L, Wimmer MA (2007) Boron functions in plants and animals: recent advances in boron research and open questions.. *In* **F Xu, H Goldbach, PH Brown, RW Bell, T Fujiwara, CD Hunt, S Goldberg, L Shi**, eds, Advances in Plant and Animal Boron Nutrition. Springer, Dordrecht, The Netherlands, pp 3–25

Hanaoka H, Uraguchi S, Takano J, Tanaka M, Fujiwara T (2014) OsNIP3;1, a rice boric acid channel, regulates boron distribution and is essential for growth under boron-deficient conditions. Plant J **78**: 890–902

Hsieh K, Huang AHC (2004) Endoplasmic reticulum, oleosins, and oils in seeds and tapetum cells. Plant Physiol **136**: 3427–3434

Hsieh K, Huang AH (2007) Tapetosomes in Brassica tapetum accumulate endoplasmic reticulum-derived flavonoids and alkanes for delivery to the pollen surface. Plant Cell **19**: 582–596

Hu J, Wang Z, Zhang L, Sun MX (2014) The Arabidopsis Exine Formation Defect (EFD) gene is required for primexine patterning and is critical for pollen fertility. New Phytol **203**: 140–154

Huang LB, Pant J, Dell B, Bell RW (2000) Effects of boron deficiency on anther development and floret fertility in wheat (*Triticum aestivum* L. 'Wilgoyne'). Ann Bot (Lond) **85**: 493–500

Hwang JH, Ellingson SR, Roberts DM (2010) Ammonia permeability of the soybean nodulin 26 channel. FEBS Lett **584**: 4339–4343

Isayenkov SV, Maathuis FJM (2008) The Arabidopsis thaliana aquaglyceroporin AtNIP7;1 is a pathway for arsenite uptake. FEBS Lett **582**: 1625–1628

Iwai H, Hokura A, Oishi M, Chida H, Ishii T, Sakai S, Satoh S (2006) The gene responsible for borate cross-linking of pectin rhamnogalacturonan-II is required for plant reproductive tissue development and fertilization. Proc Natl Acad Sci USA **103**: 16592–16597

Johanson U, Karlsson M, Johansson I, Gustavsson S, Sjövall S, Fraysse L, Weig AR, Kjellbom P (2001) The complete set of genes encoding major intrinsic proteins in Arabidopsis provides a framework for a new nomenclature for major intrinsic proteins in plants. Plant Physiol **126**: 1358–1369

Knol J, Sjollema K, Poolman B (1998) Detergent-mediated reconstitution of membrane proteins. Biochemistry **37**: 16410–16415

Kot FS (2009) Boron sources, speciation and its potential impact on health. Rev Environ Sci Biotechnol **8**: 3–28

Kreida S, Törnroth-Horsefield S (2015) Structural insights into aquaporin selectivity and regulation. Curr Opin Struct Biol **33**: 126–134

Li T, Choi WG, Wallace IS, Baudry J, Roberts DM (2011) Arabidopsis thaliana NIP7;1: an anther-specific boric acid transporter of the aquaporin superfamily regulated by an unusual tyrosine in helix 2 of the transport pore. Biochemistry **50**: 6633–6641

Li Z, Zhang P, Lv J, Cheng Y, Cui J, Zhao H, Hu S (2016) Global dynamic transcriptome programming of rapeseed (Brassica napus L.) anther at different development stages. PLoS ONE **11**: e0154039

Lindsay ER, Maathuis FJM (2016) Arabidopsis thaliana NIP7;1 is involved in tissue arsenic distribution and tolerance in response to arsenate. FEBS Lett **590**: 779–786

Liu L, Fan XD (2013) Tapetum: regulation and role in sporopollenin biosynthesis in Arabidopsis. Plant Mol Biol **83**: 165–175

Liu Q, Zhu Z (2010) Functional divergence of the NIP III subgroup proteins involved altered selective constraints and positive selection. BMC Plant Biol **10**: 256

Ludewig U, Dynowski M (2009) Plant aquaporin selectivity: where transport assays, computer simulations and physiology meet. Cell Mol Life Sci **66**: 3161–3175

Ma JF, Yamaji N (2006) Silicon uptake and accumulation in higher plants. Trends Plant Sci **11**: 392–397

Ma JF, Yamaji N (2015) A cooperative system of silicon transport in plants. Trends Plant Sci **20**: 435–442

Mathai JC, Zeidel ML (2007) Measurement of water and solute permeability by stopped-flow fluorimetry. Methods Mol Biol **400**: 323–332

Maurel C, Boursiac Y, Luu DT, Santoni V, Shahzad Z, Verdoucq L (2015) Aquaporins in plants. Physiol Rev **95**: 1321–1358

Mitani N, Yamaji N, Ma JF (2008) Characterization of substrate specificity of a rice silicon transporter, Lsi1. Pflugers Arch **456**: 679–686

Mitani-Ueno N, Yamaji N, Zhao FJ, Ma JF (2011) The aromatic/arginine selectivity filter of NIP aquaporins plays a critical role in substrate selectivity for silicon, boron, and arsenic. J Exp Bot **62**: 4391–4398

Miwa K, Fujiwara T (2010) Boron transport in plants: co-ordinated regulation of transporters. Ann Bot **105**: 1103–1108

Miwa K, Tanaka M, Kamiya T, Fujiwara T (2010) Molecular mechanisms of boron transport in plants: involvement of Arabidopsis NIP5;1 and NIP6;1. Adv Exp Med Biol **679**: 83–96

Noguchi K, Yasumori M, Imai T, Naito S, Matsunaga T, Oda H, Hayashi H, Chino M, Fujiwara T (1997) *bor1-1*, an *Arabidopsis thaliana* mutant that requires a high level of boron. Plant Physiol **115**: 901–906

O'Neill MA, Ishii T, Albersheim P, Darvill AG (2004) Rhamnogalacturonan II: structure and function of a borate cross-linked cell wall pectic polysaccharide. Annu Rev Plant Biol **55**: 109–139

Phillips R, Ursell T, Wiggins P, Sens P (2009) Emerging roles for lipids in shaping membrane-protein function. Nature **459**: 379–385

Pommerrenig B, Diehn TA, Bienert GP (2015) Metalloido-porins: essentiality of Nodulin 26-like intrinsic proteins in metalloid transport. Plant Sci **238**: 212–227

Porquet A, Filella M (2007) Structural evidence of the similarity of Sb(OH)3 and As(OH)3 with glycerol: implications for their uptake. Chem Res Toxicol **20**: 1269–1276

Rawson HM (1996) The developmental stage during which boron limitation causes sterility in wheat genotypes and the recovery of fertility. Aust J Plant Physiol **23**: 709–717

Reynolds ES (1963) The use of lead citrate at high pH as an electron-opaque stain in electron microscopy. J Cell Biol **17**: 208–212

Rigaud JL, Lévy D (2003) Reconstitution of membrane proteins into liposomes. Methods Enzymol **372**: 65–86

Rivers RL, Dean RM, Chandy G, Hall JE, Roberts DM, Zeidel ML (1997) Functional analysis of nodulin 26, an aquaporin in soybean root nodule symbiosomes. J Biol Chem **272**: 16256–16261

Roberts DM, Routray P (2017) The nodulin 26 intrinsic protein subfamily. *In* **F Chaumont, SD Tyerman**, eds, Plant Aquaporins: From Transport to Signaling. Springer International Publishing AG, Cham, Switzerland, pp 267–296

Roche JV, Törnroth-Horsefield S (2017) Aquaporin protein-protein interactions. Int J Mol Sci **18**: E2255

Sachdeva R, Singh B (2014) Insights into structural mechanisms of gating induced regulation of aquaporins. Prog Biophys Mol Biol **114**: 69–79

Sanders PM, Bui AQ, Weterings K, McIntire KN, Hsu YC, Lee PY, Truong MT, Beals TP, Goldberg RB (1999) Anther developmental defects in Arabidopsis thaliana male-sterile mutants. Sex Plant Reprod **11**: 297–322

Scott RJ, Spielman M, Dickinson HG (2004) Stamen structure and function. Plant Cell (Suppl) **16**: S46–S60

Segami S, Makino S, Miyake A, Asaoka M, Maeshima M (2014) Dynamics of vacuoles and H^+-pyrophosphatase visualized by monomeric green fluorescent protein in *Arabidopsis*: artifactual bulbs and native intravacuolar spherical structures. Plant Cell **26**: 3416–3434

Shelp BJ, Marentes E, Kitheka AM, Vivekanandan P (1995) Boron mobility in plants. Physiol Plant **94**: 356–361

Shi DQ, Yang WC (2010) Pollen germination and tube growth. *In* **EC Pua, MR Davey**, eds, Plant Developmental Biology: Biotechnological Perspectives. Springer, Berlin, pp 245–282

Shi J, Cui M, Yang L, Kim YJ, Zhang D (2015) Genetic and biochemical mechanisms of pollen wall development. Trends Plant Sci **20**: 741–753

Smith TE, Stephenson RA, Asher CJ, Hetherington SE (1997) Boron deficiency of avocado. 1. Effects on pollen viability and fruit set. *In* **RB Bell, B Rerkasem**, eds, Boron in Soils and Plants, Vol 76. Springer, Dordrecht, The Netherlands, pp 131–133

Smyth DR, Bowman JL, Meyerowitz EM (1990) Early flower development in Arabidopsis. Plant Cell **2**: 755–767

Suzuki T, Masaoka K, Nishi M, Nakamura K, Ishiguro S (2008) Identification of kaonashi mutants showing abnormal pollen exine structure in Arabidopsis thaliana. Plant Cell Physiol **49**: 1465–1477

Suzuki T, Narciso JO, Zeng W, van de Meene A, Yasutomi M, Takemura S, Lampugnani ER, Doblin MS, Bacic A, Ishiguro S (2017) KNS4/UPEX1: a type II arabinogalactan β-(1,3)-galactosyltransferase required for pollen exine development. Plant Physiol **173**: 183–205

Takano J, Yamagami M, Noguchi K, Hayashi H, Fujiwara T (2001) Preferential translocation of boron to young leaves in Arabidopsis thaliana regulated by the BOR1 gene. Soil Sci Plant Nutr **47**: 345–357

Takano J, Miwa K, Yuan L, von Wirén N, Fujiwara T (2005) Endocytosis and degradation of BOR1, a boron transporter of Arabidopsis thaliana, regulated by boron availability. Proc Natl Acad Sci USA **102**: 12276–12281

Takano J, Wada M, Ludewig U, Schaaf G, von Wirén N, Fujiwara T (2006) The *Arabidopsis* major intrinsic protein NIP5;1 is essential for efficient boron uptake and plant development under boron limitation. Plant Cell **18**: 1498–1509

Takano J, Toyoda A, Miwa K, Fujiwara T (2007) Polar trafficking and boron-dependent endocytosis of borate transporters. Plant Cell Physiol **48**: S228

Takano J, Miwa K, Fujiwara T (2008) Boron transport mechanisms: collaboration of channels and transporters. Trends Plant Sci **13**: 451–457

Takano J, Tanaka M, Toyoda A, Miwa K, Kasai K, Fuji K, Onouchi H, Naito S, Fujiwara T (2010) Polar localization and degradation of Arabidopsis boron transporters through distinct trafficking pathways. Proc Natl Acad Sci USA **107**: 5220–5225

Takano J, Yoshinari A, Luu DT (2017) **F Chaumont, SD Tyerman**, eds, Plant Aquaporins: From Transport to Signaling. Springer International Publishing AG, Cham, Switzerland

Tanaka M, Wallace IS, Takano J, Roberts DM, Fujiwara T (2008) NIP6;1 is a boric acid channel for preferential transport of boron to growing shoot tissues in *Arabidopsis*. Plant Cell **20**: 2860–2875

Tanaka N, Uraguchi S, Saito A, Kajikawa M, Kasai K, Sato Y, Nagamura Y, Fujiwara T (2013) Roles of pollen-specific boron efflux transporter, OsBOR4, in the rice fertilization process. Plant Cell Physiol **54**: 2011–2019

Tong J, Briggs MM, McIntosh TJ (2012) Water permeability of aquaporin-4 channel depends on bilayer composition, thickness, and elasticity. Biophys J **103**: 1899–1908

Tong J, Canty JT, Briggs MM, McIntosh TJ (2013) The water permeability of lens aquaporin-0 depends on its lipid bilayer environment. Exp Eye Res **113**: 32–40

Vivian-Smith A, Luo M, Chaudhury A, Koltunow A (2001) Fruit development is actively restricted in the absence of fertilization in Arabidopsis. Development **128**: 2321–2331

Wallace IS, Roberts DM (2004) Homology modeling of representative subfamilies of Arabidopsis major intrinsic proteins: classification based on the aromatic/arginine selectivity filter. Plant Physiol **135**: 1059–1068

Wallace IS, Roberts DM (2005) Distinct transport selectivity of two structural subclasses of the nodulin-like intrinsic protein family of plant aquaglyceroporin channels. Biochemistry **44**: 16826–16834

Wang S, Yoshinari A, Shimada T, Hara-Nishimura I, Mitani-Ueno N, Ma JF, Naito S, Takano J (2017) Polar localization of the NIP5;1 boric acid channel is maintained by endocytosis and facilitates boron transport in *Arabidopsis* roots. Plant Cell **29**: 824–842

Yoshinari A, Takano J (2017) Insights into the mechanisms underlying boron homeostasis in plants. Front Plant Sci **8**: 1951

Zhang Q, Chen H, He M, Zhao Z, Cai H, Ding G, Shi L, Xu F (2017) The boron transporter BnaC4.BOR1;1c is critical for inflorescence development and fertility under boron limitation in *Brassica napus*. Plant Cell Environ **40**: 1819–1833

Zhou R, Benavente LM, Stepanova AN, Alonso JM (2011) A recombineering-based gene tagging system for Arabidopsis. Plant J **66**: 712–723

Zou Z, Gong J, Huang Q, Mo Y, Yang L, Xie G (2015) Gene structures, evolution, classification and expression profiles of the aquaporin gene family in castor bean (Ricinus communis L.). PLoS ONE **10**: e0141022